Breast Cancer Research and Treatment (2023) 197:461–478
https://doi.org/10.1007/s10549-022-06819-6

PRECLINICAL STUDY

Geometric tumor embolic budding characterizes inflammatory breast cancer

Arnav P. Modi[1] · Julie P. T. Nguyen[1] · Justin Wang[1] · Jonathan S. Ahn[1] · William A. Libling[1] · Jacob M. Klein[1] · Preeanka Mazumder[1] · Sanford H. Barsky[1,2]

Received: 6 March 2022 / Accepted: 15 November 2022 / Published online: 6 December 2022

Abstract

Purpose Inflammatory breast cancer (IBC) is characterized by numerous tumor emboli especially within dermal lymphatics. The explanation remains a mystery.

Methods This study combines experimental studies with two different IBC xenografts with image algorithmic studies utilizing human tissue microarrays (TMAs) of IBC *vs* non-IBC cases to support a novel hypothesis to explain IBC's *sina qua non* signature of florid lymphovascular emboli.

Results In the human TMAs, compared to tumor features like nuclear grade (size), mitosis and Ki-67 immunoreactivity which show that IBC is only modestly more proliferative with larger nuclei than non-IBC, what really sets IBC apart is the markedly greater number of tumor emboli and distinctly smaller emboli whose numbers indicate geometric or exponential differences between IBC and non-IBC. In the experimental xenograft studies, Mary-X gives rise to tight spheroids in vitro which exhibit dynamic budding into smaller daughter spheroids whereas Karen-X exhibits only loose non-budding aggregates. Furthermore Mary-X emboli also bud dramatically into smaller daughter emboli in vivo. The mechanism that regulates this involves the generation of E-cad/NTF1, a calpain-mediated cleavage 100 kDa product of 120 kDa full length membrane E-cadherin. Inhibiting this calpain-mediated cleavage of E-cadherin by blocking either the calpain site of cleavage (SC) or the site of binding (SB) with specific decapeptides that both penetrate the cell membrane and mimic either the cleavage site or the binding site on E-cadherin, inhibits the generation of E-cad/NTF1 in a dose-dependent manner, reduces spheroid compactness and decreases budding.

Conclusion Since E-cad/NFT1 retains the p120ctn binding site but loses the α-and β-catenin sites, promoting its 360° distribution around the cell's membrane, the vacilating levels of this molecule trigger budding of both the spheroids as well as the emboli. Recurrent and geometric budding of parental emboli into daughter emboli then would account for the plethora of emboli seen in IBC.

Keywords Lymphovascular tumor emboli · IBC · Tumor embolic budding · Spheroidgenesis · Calpain-mediated proteolysis of E-cadherin · E-cadherin fragments

Abbreviations

IBC	Inflammatory breast cancer
EMT	Epithelial-mesenchymal transition
MET	Mesenchymal-epithelial transition
ERAs	Epithelial recognition algorithms
SRAs	Specific recognition algorithms
FOV	Fields of view
TMAs	Tissue microarrays
DAPI	4', 6 – Diamidino-2-phenylindole
CTCs	Circulating tumor cells
MTCs	Multicellular aggregates
E-cad	E-cadherin
FL	Full length
SC	Site of cleavage
SB	Site of binding
ctn	Catenin

✉ Sanford H. Barsky
sbarsky@mmc.edu

[1] Cancer Center and Institute for Personalized Medicine, California University of Science and Medicine, 1501 Violet Street, Colton, CA 92324, USA

[2] Department of Pathology, Anatomy and Cell Biology and the Clinical and Translational Research Center of Excellence, Meharry Medical College, 1005 Dr. D.B. Todd Jr. Boulevard, Nashville, TN 37208, USA

CAJs	Cadherin-based adherens junctions
NTF	N-terminal fragment
CTF	C-terminal fragment
ER	Estrogen receptor
PR	Progesterone receptor
ANOVA	Analysis of variance
EpCAM	Epithelial cell adhesion molecule
TNBC	Triple negative breast cancer
PCA	Principle Component Analysis
IBB	Institutional review board
IACUC	Institutional animal care and use committee
OLAW	Office of laboratory animal welfare
PDX	Patient-derived xenograft
ATCC	American Type Culture Collection

Background

The *sina qua non* of inflammatory breast cancer (IBC) is numerous lymphovascular tumor emboli within the breast and especially within overlying dermal lymphatics where they are thought responsible for the clinical signs of IBC including rubor, calor, dolor and swelling [1–3]. All molecular subtypes of IBC exhibit this unifying phenotype whose mechanism remains unknown [4].

Previous studies by us and others using human xenograft models of inflammatory breast cancer and related cell lines have shed some light on the mechanisms responsible for the genesis of tumor clumps and derived emboli in the metastatic cascade of IBC [5–10]. In these studies membrane E-cadherin is an important adhesion molecule and its overexpression responsible for the tumor clumping that occurs [10–12]. Although E-cadherin generally is also considered a tumor suppressor gene / protein in tumor invasion and metastasis whose loss contributes to epithelial-mesenchymal transition (EMT) [13–15], in the setting of the tumor cell clump or the lymphovascular embolus of IBC, E-cadherin acts more like a dominant oncogene. [16–18]

However, these previous observations do not explain the plethora of emboli that occur in IBC, especially within dermal lymphatics. Certainly E-cadherin overexpression while contributing to the tumor cell clump and the tumor cell embolus can not alone account for the plethora of lymphovascular emboli observed in IBC.

For these reasons we sought explanations that might be responsible for this unique phenotype of IBC. We had collected a number of cases of human breast cancer of all types including IBC and non-IBC that were available to study through TMA digital algorithmic image analysis for detailed human observational studies. We also had pooled microdissected emboli available from the IBC cases. We had also established two contrasting xenograft models of IBC, Mary-X and Karen-X, to use in experimental studies to explain the unique phenotype of florid lymphovascular emboli observed in IBC.

Methods

Institutional approvals and initial establishment of the xenografts

Collection and use of human tissues from patients with breast cancer including non-IBC as well as IBC cases, completely anonymized, was approved by The Ohio State University Cancer Institutional Review Board (IRB) under protocol 2006C0042.

Both Mary-X and Karen-X were derived from patients with a biopsy proven diagnosis of IBC in the 1990's and made into transplantable xenografts. Patient consents were obtained and studies were conducted under the UCLA's Human Subject Protection Committee and the Chancellor's Animal Research Committee (Certification 95–127-11). Mary-X was derived from a biopsy of primary IBC whereas Karen-X was derived from a biopsy of a hepatic metastases. Mary-X exhibited triple (ER, PR and Her-2/neu) negativity whereas Karen-X was weakly estrogen receptor (ER) positive. Both xenografts have been phenotypically stable for over 25 years of passage.

Both patient-derived xenografts (PDX) initially were directly implanted into the 4^{th} mammary fat pad of both nude as well as Scid mice. When tumors emerged, they were both serially transplanted as well as placed in suspension culture. Both Mary-X and Karen-X spontaneously formed spheroids. The spheroids of Mary-X were tight and highly dense whereas the spheroids of Karen-X appeared as loose aggregates. Neither line formed monolayers on either plastic or fibronectin, vitronectin or collagen coated plastic. 10^3 spheroids (100μ diameter) with each spheroid consisting of approximately 10^3 cells or a total of 10^6 cells were also injected into the 4^{th} mammary fat pad. In the case of both serially transplants or injected spheroids, tumors emerged which illustrated a stable phenotype and a characteristic histopathology. Over the years the sites of injection in the mice were varied to include the other mammary fat pads and non-orthotopic sites. Irrespective of the site of injection, both the phenotypes, histopathology and biology of Mary-X and Karen-X remained constant with passage. In previous studies with Mary-X, sorted signal cells, eg. stem cells, were also obtained on the basis of several stem cell markers and reinjected with the maintenance of a stable phenotype [19, 20]. Cells lacking stem cell markers were not tumorigenic.

Continuing animal studies were approved by The Ohio State University's Institutional Animal Care and Use Committee (IACUC), protocol 2007A0218 and by The Ohio State University's Institutional Biosafety Committee, protocol

2007R0057. Additional animal studies were approved by the University of Nevada's School of Medicine and the Nevada Cancer Institute's IACUC, protocols 00439 and 00440 when the corresponding author of this study was affiliated with these previous institutions. Final animal studies were conducted under an Interinstitutional Agreement between the California University of Science and Medicine and Anticancer, Inc. using the latter's IACUC protocol D16-00503 and Office of Animal Welfare (OLAW) A3873-01.

ATCC patent deposits and cell identification

Mary-X and its in vitro derived spheroids were deposited in the American Type Culture Collection (ATCC) cell repository (Manassas, VA) as PTA-2737 and PTA-27376, respectively, and recently verified and re-verified to be both novel and human in origin (STRA4993). Likewise Karen-X and its in vitro derived spheroidal aggregates were deposited in the ATCC cell repository as PTA-126676 and PTA-126677 respectfully and recently verified to be both novel and human in origin (STRA4980). Mary-X is a well-known transplantable model of inflammatory breast cancer and has been used in numerous previous studies [19–21]. Karen-X has not previously been reported, although it has been ATCC deposited.

Observational studies

Cases of IBC

2000 cases of non-IBC and 100 cases of IBC were randomly selected from a database and The Ohio State University's Information Warehouse and anonymized.

TMA construction

Multiple 2-mm tissue cores of tumor from each paraffin-embedded donor block (average of 10 cores / block) were arrayed into recipient TMA blocks, each of which contained 100 cores. All retrieved cases were processed in this manner.

Histological and immunohistochemistry studies

Primary antibodies used included rat anti-human Ki-67 (DakoCytomation, Carpinteria, CA), D2-40 anti-podoplanin (clone D2-40, Dako, catalog number M3619) and anti-CD31 (rabbit polyclonal, Spring Bioscience, catalog number E11114). The appropriate secondary antibodies were linked to an identifying chromogen.

Imaging analysis and quantitation of Ki-67 index, mitotic count, nuclear size (grade) and lymphovascular tumor emboli (embolic density, shape and size)

Our specific TMA algorithms carried out virtual alignment, image processing, and the application of the epithelial recognition algorithms (ERAs) and specific recognition algorithms (SRAs), the latter based upon immunocytochemical studies that quantitated nuclear Ki-67 immunoreactivity [22–25]. Additional specific morphological algorithms included a mitosis algorithm [26], a nuclear grade (size) algorithm [27], and epithelial clustering algorithms quantitating embolic density and measuring embolic shape (elongation ratio: short/long axis) and size (perimeter) utilizing ImageJ software [28]. Image acquisition by either the Aperio ScanScope T2 System (Aperio, Vista, CA) or the iSCAN System (BioImagene, Inc, Cupertino, CA.) produced equivalent results. The imaging apparatus captured sequential fields of view (FOV) from each core to cover the core in its entirety. Modes and means ± standard deviations (SD) were calculated for all these measurements. All experiments were performed in quintuplicate.

Experimental studies

Continued xenograft studies

Athymic (nude) mice as well as Scids on BALB/c backgrounds, 4 week old females, purchased from Anticancer, Inc. (San Diego, CA) were derived from their respective breeding colonies. Mary-X and Karen-X were grown as transplantable xenografts. At selected intervals ranging up to 4 months, the mice were euthanized with 25 mg/ml ketamine, 2 mg/ml xylazine and acepromazine and subjected to necropsy. Routine histological and immunocytochemical studies were carried out on excised tumors. Antibodies used included biotinylated E-cadherin rabbit mAb (24E10) (Santa Cruz Biotechnology, Santa Cruz, CA) which recognized both full length E-cadherin (E-cad/FL) and its E-cadherin/N-terminal fragment1 (E-cad/NTF1), followed by a labeled Streptavidin–Biotin Complex (Santa Cruz Biotechnology, Santa Cruz, CA). DAB chromogen was used to develop the brown color.

In vitro *studies*

Both Mary-X and Karen-X were placed in culture and 2 mm thick slices of each tumor were minced in RPMI media with 10% fetal calf serum giving rise to liberated loose aggregates in suspension culture. These aggregates were then passed through cell strainers whose pore sizes ranged from 40 to 500 µm. The morphology of the aggregates were observed over the next 24–72 h by phase contrast microscopy using

the CytoSMART Lux2 (CytoSmart Technologies B.V. The Netherlands).

Confocal single and double label immunofluorescence experiments on Mary-X and Karen-X

Mary-X spheroids and Karen-X loose aggregates were subjected to single label immunofluorescence studies using Alexa Fluor 488-conjugated 24E10 (#3199) (Cell Signaling Technology, Inc.) which recognized both E-cad/FL as well as E-cad/NTF1. In order to immobilize the spheroids and loose aggregates, glass-bottom dishes were coated with Cell-TEK adhesive. The adherent spheroids were then fixed with 4% paraformaldehyde, after permeabilizing with TX-100 and blocking with normal goat serum. After washing with PBS 4–5 times, each for 10 min, the spheroids and aggregates were incubated with 24E10. The dishes were finally mounted with Vectorshield mounting medium with DAPI (#H-1200) (Vector Laboratories) and viewed with a Olympus Fluoview-1000 confocal scanning system.

Mary-X and Karen-X were also subjected to double label immunofluorescence studies. Double label immunofluorescence experiments were carried out using the following combinations of antibodies: Alexa Fluor 488-conjugated 24E10 which recognized both E-cad/NTF1 as well as E-cad/FL and goat polyclonal antibody to mouse podoplanin or CD31 (R&D Systems, Inc.) which recognized murine lymphatics or blood vessels followed by Alexa Fluor 594-conjugated donkey anti-goat (#A11058) (Invitrogen, Inc.). Tumor emboli were recognized by E-cadherin positivity surrounded by circumferential podoplanin (lymphatics) or CD31 positivity.

Isolation of Circulating Tumor Cells (CTCs) using EpCAM microbeads

CTCs were isolated from 10 mice each harboring the Mary-X and Karen-X xenografts. Blood from mice harboring at least 2 cm in diameter tumors were obtained by cardiac puncture and CTCs isolated with Epithelial Cell Adhesion Molecule (EpCAM) microbeads [29].

Laser capture microdissection

Frozen Sects. (8 μm) of Mary-X and human IBC cases were obtained, fixed in 70% ethanol, stained with hematoxylin and progressively dehydrated. Tumor emboli and non-embolic solid areas of Mary-X and human IBC cases were microdissected using a Pixcell II Laser Capture Microdissection 788 Laboratory System (Arcturus, Inc., Mountain View, CA) and stored at − 80 °C. 100 microdissected emboli /case from 10 cases were pooled together in individual aliquots. A total of 20 aliquots were prepared and stored for future studies.

Preparation of protein lysates and western blot analysis

The xenografts and laser-captured microdissected and pooled frozen IBC emboli were lysed using ice-cold RIPA lysis buffer (Pierce Biotechnology, Inc, Rockford, IL). For western blot analysis, boiled protein was loaded onto a 4–12% precast gradient gel (Invitrogen, Inc.), transferred to nitrocellulose membranes (Bio-rad, Hercules, CA) and incubated with either E-cadherin rabbit mAb (24E10) or rabbit anti-human ectodomain E-cadherin (H108) (Santa Cruz Biotechnology, Santa Cruz, CA) followed by anti-rabbit IgG, HRP-linked antibody (Cell Signaling Technology Inc., Danvers, MA). Rabbit mAb (13E5) was used to a housekeeping protein, ACTB. Bound antibodies were detected by a chemiluminescent detection system (West Femto) (Pierce Biotechnology, Inc.) according to the manufacturer's instructions. The relative intensity of the bands was determined by densitometric analysis.

Synthesis, labelling and use of SC and SB decapeptides

The calpain cleavage and binding sites on full length E-cadherin were used as a template to design mimicking decapeptides to block calpain cleavage and binding. Two decapeptides: the site of cleavage (SC) peptide: DARPEVTRND and the site of binding (SB) peptide: GGEEDQDFDL were purchased and used in concentration ranges of 50 nM to 50 μM (ThermoFisher Scientific, Inc., Waltham, MA). The same decapeptides were also obtained labelled, respectively, with Alexa Fluor 488 and Alexa Fluor 594 at their NH_2-terminal ends and used in the same concentration ranges. Both the labelled and unlabelled decapeptides were studied in vitro for their abilities to penetrate into the spheroidal aggregates of both Mary-X and Karen-X, transgress the cell membrane, block E-cad/NTF1 generation and affect spheroidgenesis. Specifically dose response effects of the decapeptides on E-cad/NTF1 generation and effects on both spheroid disadherence and budding were observed and recorded. Decapeptides with random amino acid sequences in the same concentration ranges of 50 nM–50 μM served as negative controls in both the studies of E-cad/NTF1 generation as well as spheroidgenesis.

Statistical analysis

For Ki-67 index, mitotic count and nuclear grade (size) and measurements of embolic density, shape (elongation ratio) and size, both modes and means ± SD values were

determined. All experiments were performed in quintuplicate and representative results depicted showing %cases, modes or means ± standard deviations. All stated or calculated differences imply differences of statistical significance, assessed by the two tailed students *t* test as well as analysis of variance (ANOVA).

Results

Observational studies

In the human TMA studies, compared to other tumor features like nuclear grade (size), mitosis and Ki-67 immunoreactivity which showed that IBC is only modestly more proliferative with larger nuclei than non-IBC, what really distinguished IBC was the markedly greater number of tumor emboli and distinctly smaller emboli (Fig. 1). IBC cases compared to non-IBC cases showed a modestly greater Ki-67 mean index ($p = 0.05$) (Fig. 1A), a modesty higher mean mitotic count ($p = 0.05$) (Fig. 1B) and a modestly increased mean nuclear grade ($p = 0.05$) (Fig. 1C) but the distribution of these tumor features showed considerable overlap. In contrast, mean embolic density in IBC dwarfed non-IBC by a factor of 100-fold ($p = 0.0001$) (Fig. 1D). Furthermore although the overall mode and mean shape of the emboli in IBC *v* non-IBC did not differ ($p = 0.5$) (Fig. 1E), the modal and mean size of the IBC emboli were significantly smaller ($p = 0.01$) (Fig. 1F).

Experimental studies

Initial xenograft studies

Mary-X grew equally well in both athymic (nude) mice as well as Scids as a transplantable xenograft (Fig. 2A). Mary-X exhibited a stable phenotype for over 25 years. Mary-X grew in a nodular fashion with islands of tumor cells embedded within a murine fibrovascular matrix (Fig. 2B). The nodules of Mary-X expressed strong membrane E-cadherin immunoreactivity (Fig. 2D). Mary-X gave rise to large numbers of CTCs (Fig. 2F: inset) which measured out at 10–15 cells / 100 µl blood as well as distal metastases including pulmonary metastases (Fig. 2F). These metastases also strongly expressed E-cadherin.

Karen-X, in contrast, grew only in Scids as a transplantable xenograft (Fig. 2). Karen-X also exhibited a stable phenotype for over 25 years. Karen-X exhibited a significantly longer latency than Mary-X but once a tumor emerged exhibited a similar rate of growth (Fig. 2A). Karen-X was similar to Mary-X histologically (Fig. 2C). Karen-X also expressed E-cadherin membrane immunoreactivity which overall was less intense and less circumferential (Fig. 2E) than that expressed in Mary-X. In contrast to Mary-X, Karen-X did not generate CTCs (Fig. 2G: inset) or metastases (Fig. 2G).

In vitro *studies*

Mary-X and Karen-X exhibited markedly different in vitro properties when grown in suspension culture (Fig. 3). When their respective xenografts were excised and minced in culture, both initially gave rise to loose tumor aggregates. After 24–48 h, the Mary-X aggregates tightened to form high density spheroids (Fig. 3A) whereas the Karen-X aggregates remained loosely associated and did not tighten (Fig. 3G). After an ensuing 24 h–96 h period, the Mary-X spheroids exhibited both partial budding as well as complete budding. We counted over 1000 spheroids over a 96 h period and observed partial budding in 15 ± 5% and complete budding in 5 ± 3%. Partial budding was defined as budding that had not yet completely separated and complete budding was defined as full separation with the appearance of daughter spheroids. When observed with time-lapsed photography, the budding of Mary-X spheroids was rapid and quite dynamic, occurring over minutes (Supplement 1). In this time-lapsed photography, one parent spheroid divided into two and the two divided into four, illustrating a geometric progression. Still images from the time-lapsed video demonstrate this unique budding of Mary-X spheroids (Fig. 3B-3F). Mary-X budding gave rise to daughter spheroids which were smaller in size (Fig. 4A) which nevertheless expressed strong E-cadherin immunoreactivity (Fig. 4B). In contrast, Karen-X spheroids did not bud over time in suspension culture (Supplement 2). Still images of the Karen-X spheroids confirmed the lack of budding and their persistence as loose aggregates (Fig. 3G). Neither Mary-X nor Karen-X ever attached or grew as monolayers even when grown on fibronectin or vitronectin-coated dishes (data not shown). Furthermore, both Mary-X and Karen-X spheroids grew only minimally in suspension culture and then underwent a growth arrest. Initially, Ki-67 immunoreactivity in both Mary-X and Karen-X spheroids was high but then decreased over several weeks in culture. In contrast both the Mary-X and the Karen-X xenografts grew fairly rapidly with a relatively high Ki-67 index (> 50%). Yet despite the growth latency in vitro, both Mary-X and Karen-X spheroids were fully tumorigenic when reinjected into mice, even after 6 months in culture.

Additional xenograft studies

Double label immunofluorescence studies of the excised Mary-X xenograft showed florid tumor embolic lymphovascular budding (Fig. 4C). In contrast the Karen-X xenograft showed no lymphovascular invasion and no budding (data

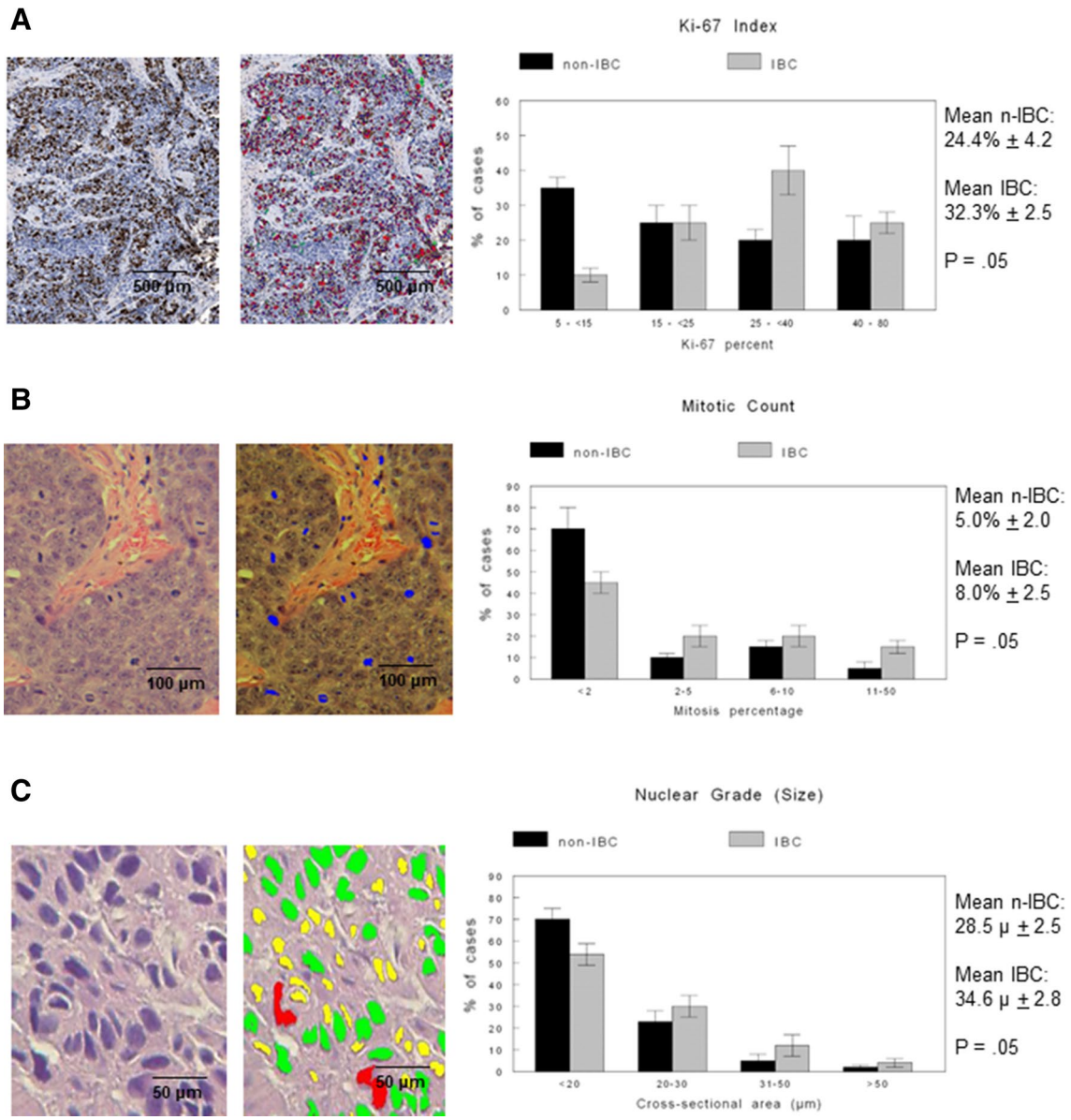

Fig. 1 Image and algorithmic analyses of multiple histological and immunocytochemical parameters in IBC *v* non-IBC human cases. **A** Ki-67 immunoreactivity (left), specific algorithmic recognition (middle) and Ki-67 index quantitation (right) in IBC *v* non-IBC are illustrated. **B** Mitosis histology (left), specific algorithmic recognition (middle) and mitotic count determination (right) in IBC *v* non-IBC are illustrated. **C** Nuclear histology (left), specific algorithmic quantitation (middle) and nuclear grade (size) distribution (right) in IBC *v* non-IBC are illustrated: yellow, < 20 µm; green, 20–30 µm; red, 31–50 µm. **D** Tumor embolic histology (left) and density determinations (right) in IBC *v* non-IBC are illustrated. **E** Tumor embolic histology (left) and algorithmic imaging shape determinations (right) in IBC *v* non-IBC are illustrated. **F** Tumor embolic imaging (left) and algorithmic perimeter determinations (right) in IBC *v* non-IBC are illustrated. Scale bars are provided. For each of these parameters, the graph depicts %cases, modal values (plotted) and calculated means ± SD. Differences of significance are depicted. All experiments were performed in quintuplicate

not shown). The parental tumor embolic budding of Mary-X gave rise to a dramatic geometric increase in the number of smaller tumor emboli within lymphovascular channels (Fig. 4C, D). Both parental and daughter tumor emboli retained strong membrane E-cadherin immunofluorescence (Fig. 4C, D). Non-embolic tumoral areas of Mary-X showed no evidence of budding.

Studies of Mary-X and Karen-X E-cadherin proteolysis

Our previous Mary-X studies had demonstrated the transcriptome equivalence of xenograft-generated spheroids with the lymphovascular emboli in mice with both structures also demonstrating E-cadherin overexpression and specific proteolytic processing with calpain and other

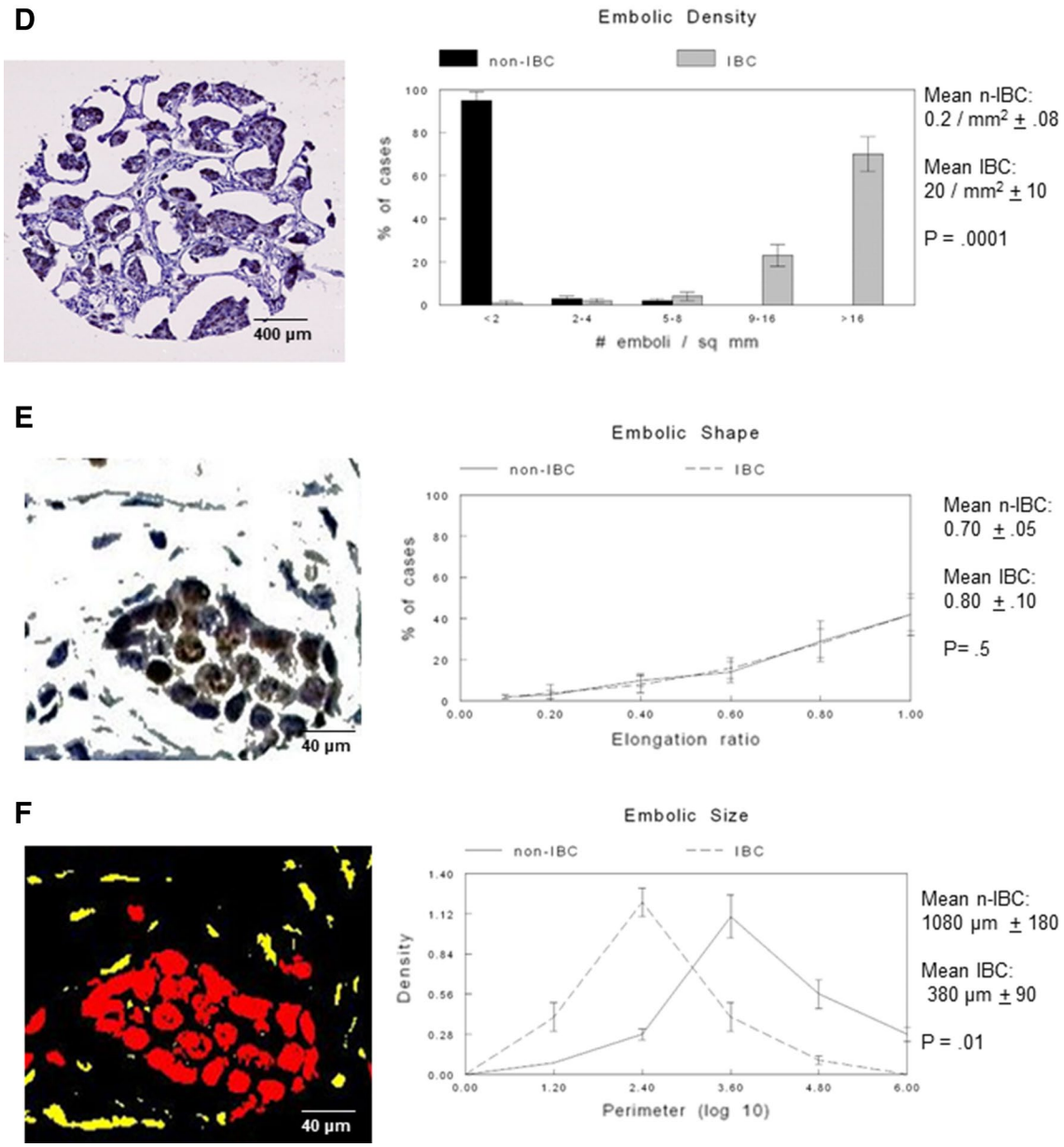

Fig. 1 (continued)

proteases, producing a number of specific E-cadherin fragments including Ecad/NTF1-4 and Ecad/CTF1-4 [21, 30]. Western blots with either E-cadherin rabbit mAb (24E10) or rabbit anti-human ectodomain E-cadherin (H108) in the present study confirmed the high levels of both E-cad/FL as well as E-cad/NTF1 in the Mary-X spheroids but absent E-cad/NTF1 in the Karen-X aggregates (Fig. 5A). Laser capture microdissected pooled lymphovascular tumor emboli from patients (100 emboli / case from 10 cases with IBC) (Fig. 5B) showed similarly high levels of both E-cad/FL as well as E-cad/NTF1 (Fig. 5C).

Because calpains, as intracellular proteases, have many different actions on many different targets, blocking calpains with calpastatin would not be expected to solely block only the cleavage of E-cadherin and the generation of its E-cad/NTF1 fragment. So in the present study, we used specific oligopeptides (decapeptides) that mimicked, respectively, either calpain's site of cleavage (SC) or site of binding (SB) on the full length E-cadherin molecule. Both decapeptides by Western blot significantly inhibited the generation of E-cad/NTF1 in a dose-dependent manner confirmed by densitometric analysis (Fig. 6A). No effects on the generation of E-cad/NTF1 were observed in the Karen-X spheroids likely

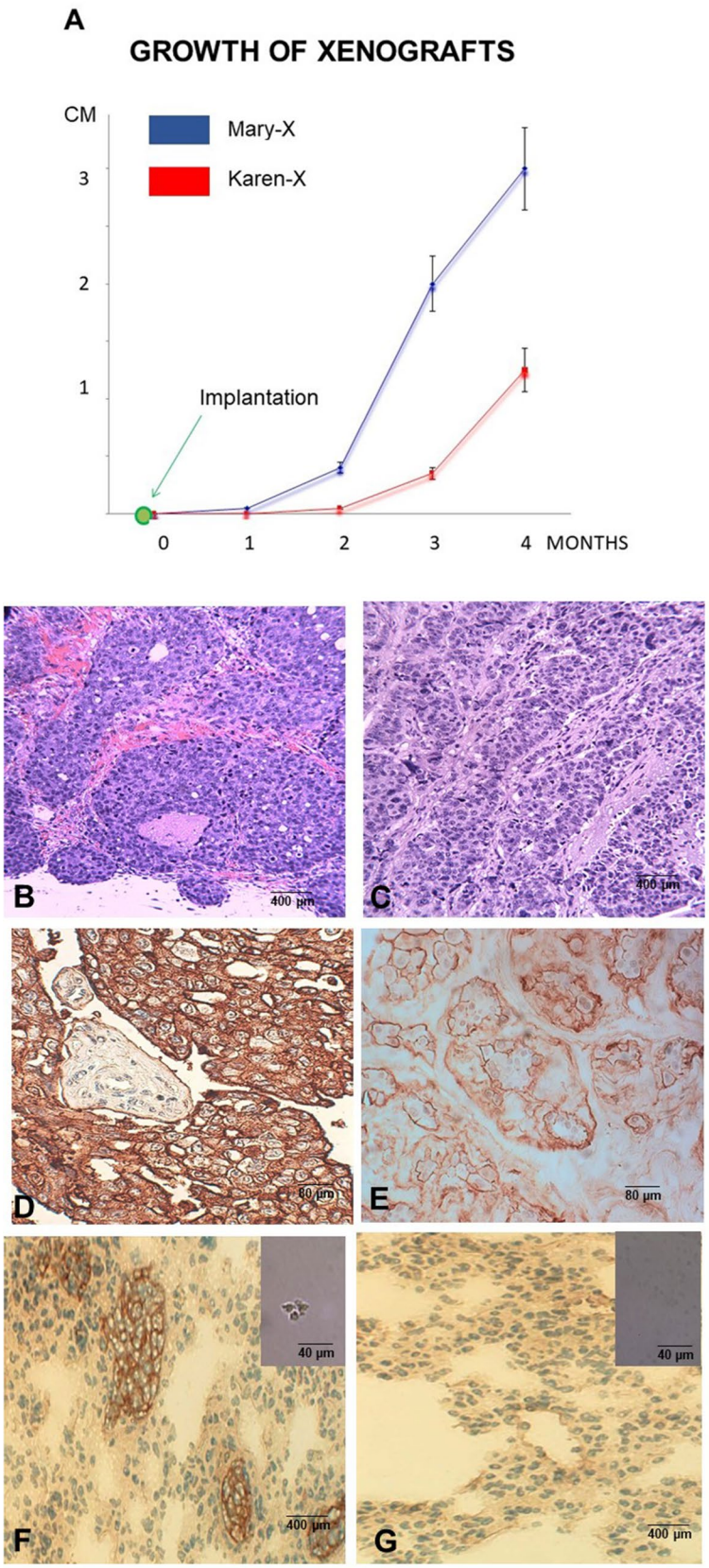

Fig. 2 Xenograft Properties. **A** The growth of Mary-X and Karen-X are depicted. Each time point displays the mean ± standard deviation of 10 mice. Routine histology of Mary-X (**B**) and Karen-X (**C**) shows similar nodular islands of tumor cells. E-cadherin immunocytochemistry shows more intense and more circumferential membrane immunoreactivity in Mary-X (**D**) compared to Karen-X (**E**). Mary-X gives rise to E-cadherin positive pulmonary metastases (**F**) as well as CTCs (F: inset) whereas Karen-X lacks both (**G**, G: inset). Scale bars are provided.

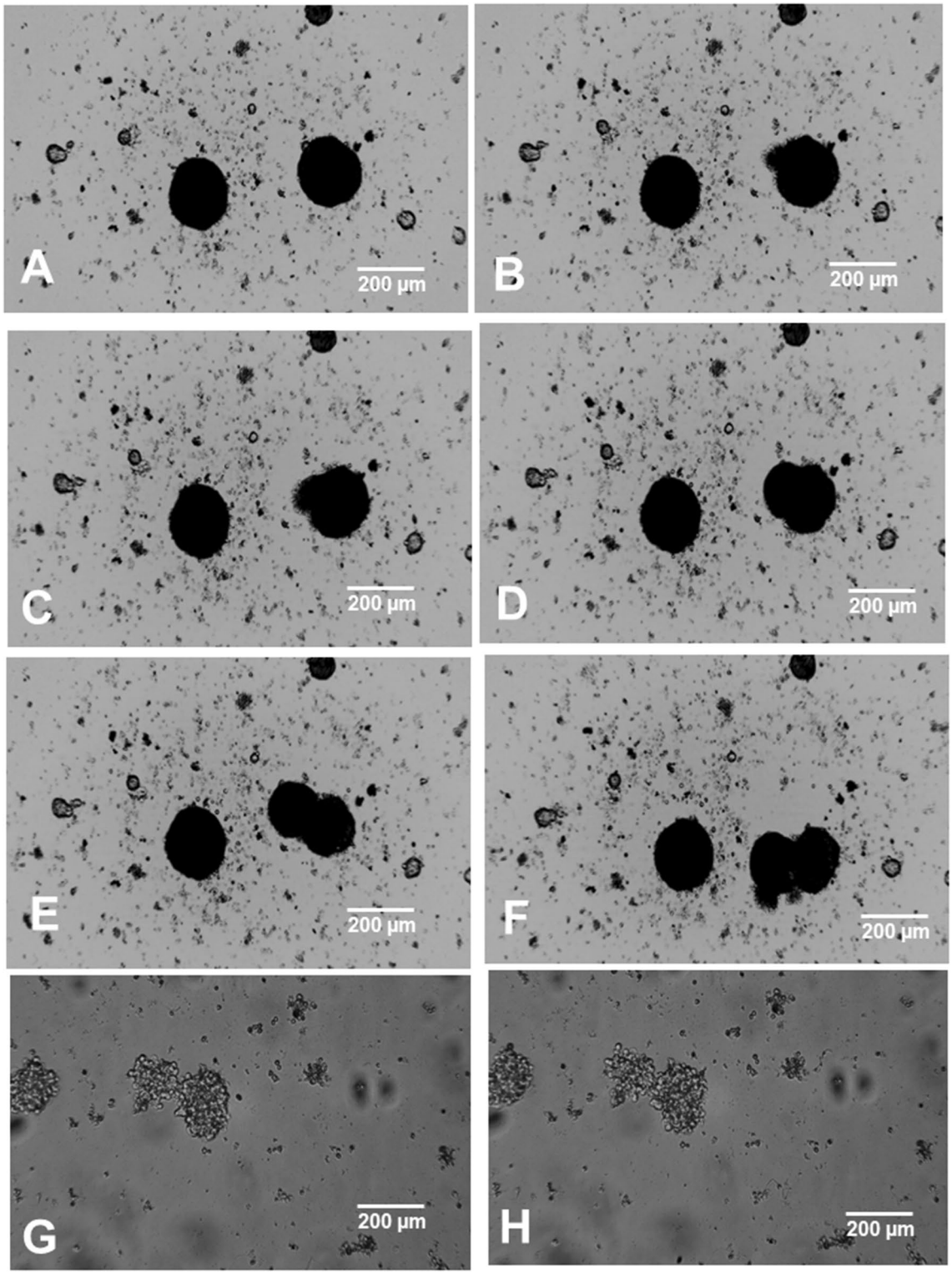

Fig. 3 In Vitro Clump Properties. Time-lapsed phase contrast microscopy depicts Mary-X spheroids growing in suspension culture as tight aggregates which completely bud into daughter spheroids (Supplement 1). Still images of this dynamic budding are depicted (**A**–**F**). In contrast, Karen-X spheroids remain as loose aggregates which do not bud (Supplement 2). Still images confirm this absence of budding (**G**, **H**)

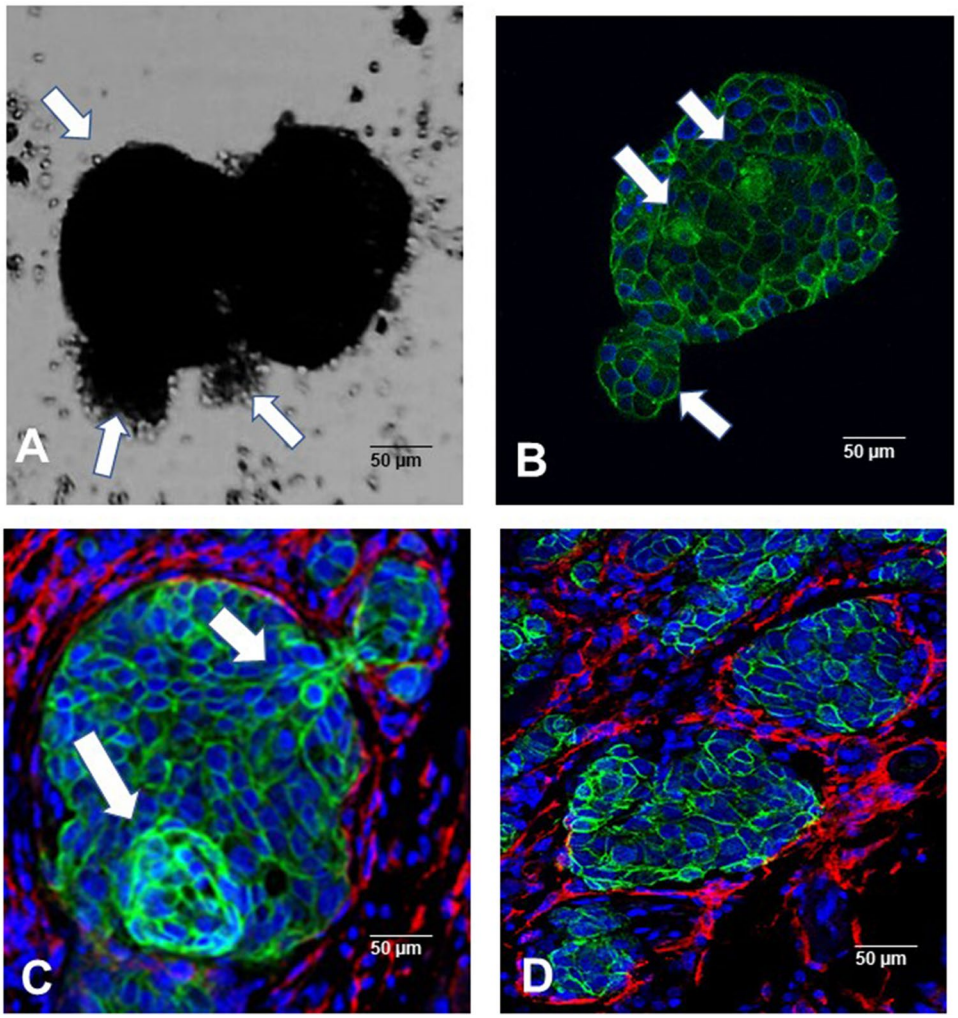

Fig. 4 Complete Budding both In Vitro and In Vivo. Complete budding of Mary-X with phase contrast (**A**) and single label E-cadherin immunofluorescence (**B**). E-cadherin immunoreactivity remains intense even at the points of the budding (**B**). DAPI was used as a nuclear counterstain. White arrows indicate budding points. Time-lapse photography confirms the dynamics of the budding process (Supplement 1). Double label immunofluorescent studies demonstrate tumor emboli exhibiting green immunofluorescence within podoplanin-positive lymphovascular channels exhibiting red immunofluorescence with DAPI used as a nuclear counterstain. Dramatic complete embolic budding is also observed in vivo (**C**). E-cadherin immunoreactivity remains intense even at the points of the budding. White arrows indicate budding points. As a result of this geometric budding, large numbers of tumor emboli are propagated (**D**). Scale bars are provided

because Karen-X spheroids did not generate E-cad/NTF1 de novo (Fig. 6B).

Using the same SC and SB decapeptides as before but now labelled, respectively, with Alexa Fluor 488 and Alexa Fluor 594, the decapeptides were administered to the Mary-X spheroids**.** Each peptide singly and in combination penetrated the spheroids (Fig. 6C). The effects on the Mary-X spheroids were significant in terms of both increased disadherence ($p < 0.05$), decreased partial and complete budding ($p < 0.05$) (Fig. 6D). The effects of the SB peptide were greater than the inhibitory effects of the SC peptide on E-cad/NTF1 generation ($p < 0.05$) but both peptides promoted disadherence, and decreased budding equally. The effects of the two peptides in combination were synergistic on inhibition of E-cad/NTF1 generation ($p < 0.05$), increased disadherence and decreased budding ($p < 0.05$). There were no measurable effects of these decapeptides on the loose aggregates of Karen-X (data not shown). Decapeptides with random amino acid sequences which served as negative controls in both the E-cad/NFT1 inhibition experiments as well as in the studies of spheroidgenesis and budding exerted no effects.

Discussion

IBC is the deadliest type of human breast cancer that presents with florid tumor emboli especially involving overlying dermal lymphatics [1–5]. These lymphovascular tumor emboli also reoccur locally, making skin-sparing and breast-conserving surgery not a usual option. [31–35]

In our human TMA studies, our detailed image analysis with artificial intelligence algorithms demonstrated what really set IBC apart was the markedly greater number of tumor emboli and distinctly smaller emboli whose numbers exhibited dramatic geometric or exponential differences. That novel observation together with our in vitro / murine in vivo observations supported our hypothesis that IBC

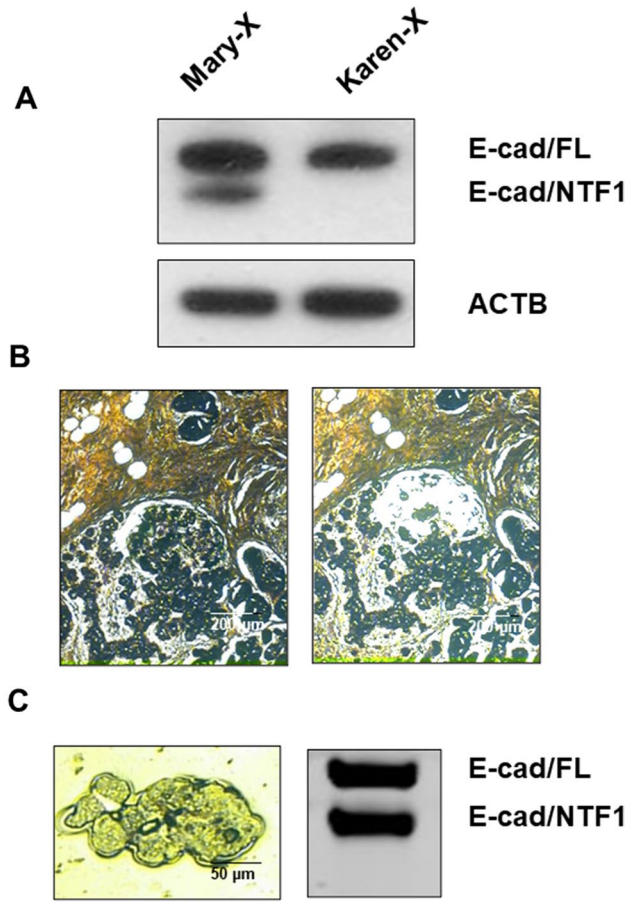

Fig. 5 Expression of E-cad/FL and E-cad/NTF1. Western blot using H108 reveals both E-cad/FL and E-cad/NTF1 in Mary-X but essential absence of E-cad/NTF1 in Karen-X (**A**). Laser capture microdissection of tumor emboli (**B**) from cases of IBC also confirm the presence of E-cad/NTF1 by Western blot (**C**)

emboli bud into daughter and *smaller* emboli in patients. These emboli likely were the source of numerous CTCs and metastases [36, 37] although more recent studies have questioned whether the density of lymphovascular emboli necessarily correlate with numbers of CTCs [38]. The budding of Mary-X in vitro was dynamic, dramatic and fairly rapid (occurring in minutes).

We used only two xenografts, Mary-X and Karen-X, xenografts we originated and established in immunodeficient mice because although there have a number of other aggressive triple negative breast cancer (TNBC) lines and xenografts reported in the literature and studied, we are not aware of any published studies that show that they spontaneously form spheroids in suspension culture or bud or form tumors as xenografts that also bud into daughter emboli. In our study we are attempting to take advantage of the fact that one of our PDX models, Mary-X still metastasizes, forms lymphovascular emboli through budding whereas our other model, Karen-X, neither metastasizes, forms lymphovascular emboli nor buds, arguing that these three properties are causally related. We do plan in future studies to study both Mary-X and Karen-X in mice whose immune system has been restored and humanized. [39, 40]

In a previous study [21] we reported the calpain-mediated cleavage in Mary-X and the generation of E-cad/NTF1. In that study and in our present work, we note that calpain cleaves E-cadherin at amino acid site: 782 and the size fragments expected from that cleavage are 100 kDa for the NH2-terminal end and 10 kDa for the COOH terminal end. We used two different E-cadherin antibodies, H108 and 24E10 that recognized amino acid sites: 695–701 and 778–781, respectively, to distinguish the different cleavage products produced by the different proteases including calpain (Fig. 7A).

Our current work significantly advances this observation in several ways: it shows that the lymphovascular emboli of Mary-X exhibit complete budding both in vitro by time-lapsed photography and in murine studies with the generation of completely intact and *smaller* daughter emboli and that this budding can be inhibited in vitro by blocking calpain cleavage of E-cadherin and the generation of E-cad/NTF1 with decapeptides that mimic either the cleavage site or the binding site on E-cadherin in a dose-dependent manner.

Metastases is a complex process regulated by multiple determinants so just because calpain-mediated cleavage of E-cadherin into E-cad/NTF1 that contributes to a budding phenomenon is observed in IBC, it does not follow necessarily that reduced calpastatin which would contribute to increased calpain or increased calpain alone would be responsible for increased metastases and poor survival across the board if the rate-limiting steps of metastasis of other cancers including non-IBC were governed by other pathways such as adhesion or proliferation. Furthermore while certainly our studies suggest that E-cadherin/NTF1 could be a marker of poor prognosis and this should be studied, other markers characteristic of other pathways could well be confounding in other tumor types. For starters, we do plan to measure E-cad/NTF1 levels in lymphovascular emboli retrieved by laser capture microdissection in a cohort of just IBC cases and see whether the levels predict disease-free survival and overall survival.

In our study we are distinguishing geometric budding of emboli from the phenomenon that triggers initial lymphovascular invasion in the first place, which, in itself remains unexplained. The recognition of the lymphovascular embolus as an entity unto itself has catalyzed larger observations that many cancers invade and metastasize as clumps or clusters [41–48]. Up until relatively recently, most scientists considered cancers to metastasize as single cells and their increased locomotion and degradation of the extracellular matrix with subsequent lymphovascular invasion as a

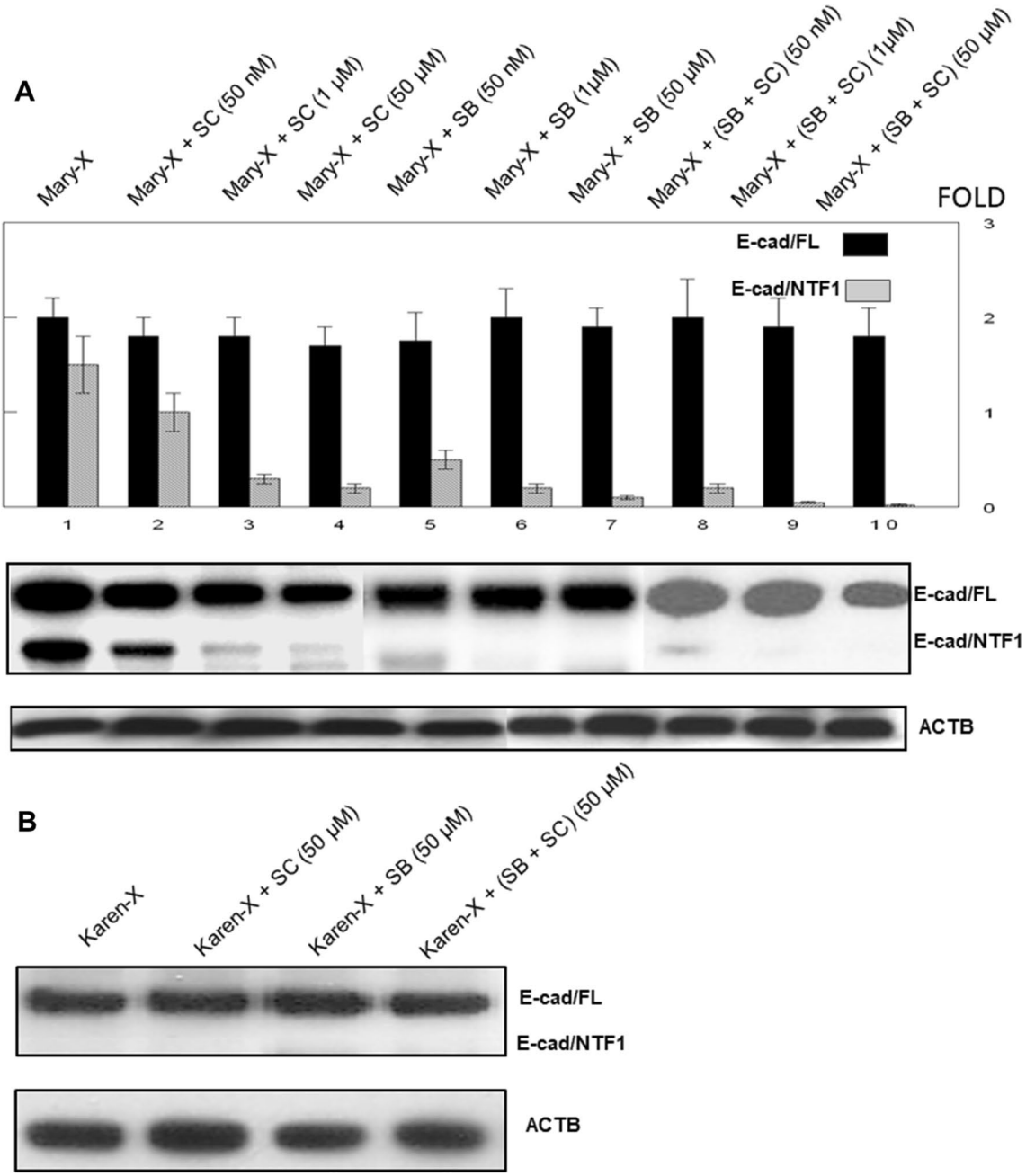

Fig. 6 Effects of SC and SB decapeptides. Dose response of SC and SB decapeptides on E-cad/NTF1 generation in Mary-X spheroids (**A**). Each decapeptide singly and in combination was effective at blocking calpain generation of E-cad/NTF1 illustrated by Western blots. In Karen-X spheroids, since there was no or negligible E-cad/NTF1, these decapeptides exerted no effects (**B**). In vitro delivery and action of fluorescently labelled decapeptides on tumor clumps are depicted (**C**). SC peptide labelled with Alexa Fluor 488 (green fluorescence) (top row, left panel) and the SB peptide labelled with Alexa Fluor 594 (red fluorescence) (top row, center panel) both singly and in combination (yellow fluorescence) (top row, right panel), penetrated the cell membranes (bottom row, left and right panels) and caused increased disadherence and decreased budding (**D**). Effects of both decapeptides were synergistic. Scale bars are provided

manifestation of so called epithelial-mesenchymal transition (EMT) [13–15]. Models epitomizing this phenomenon in the breast included infiltrating lobular cancers where cells lose E-cadherin expression and infiltrate as single cells. [49, 50]

The study of tumor cell clumps or clusters became important not only in vivo but also in vitro because tumor clumps in suspension culture provided 3D models which were uniformly superior to 2D monolayer cultures of cancer cell lines. In vitro 3D models were thought to better recapitulate

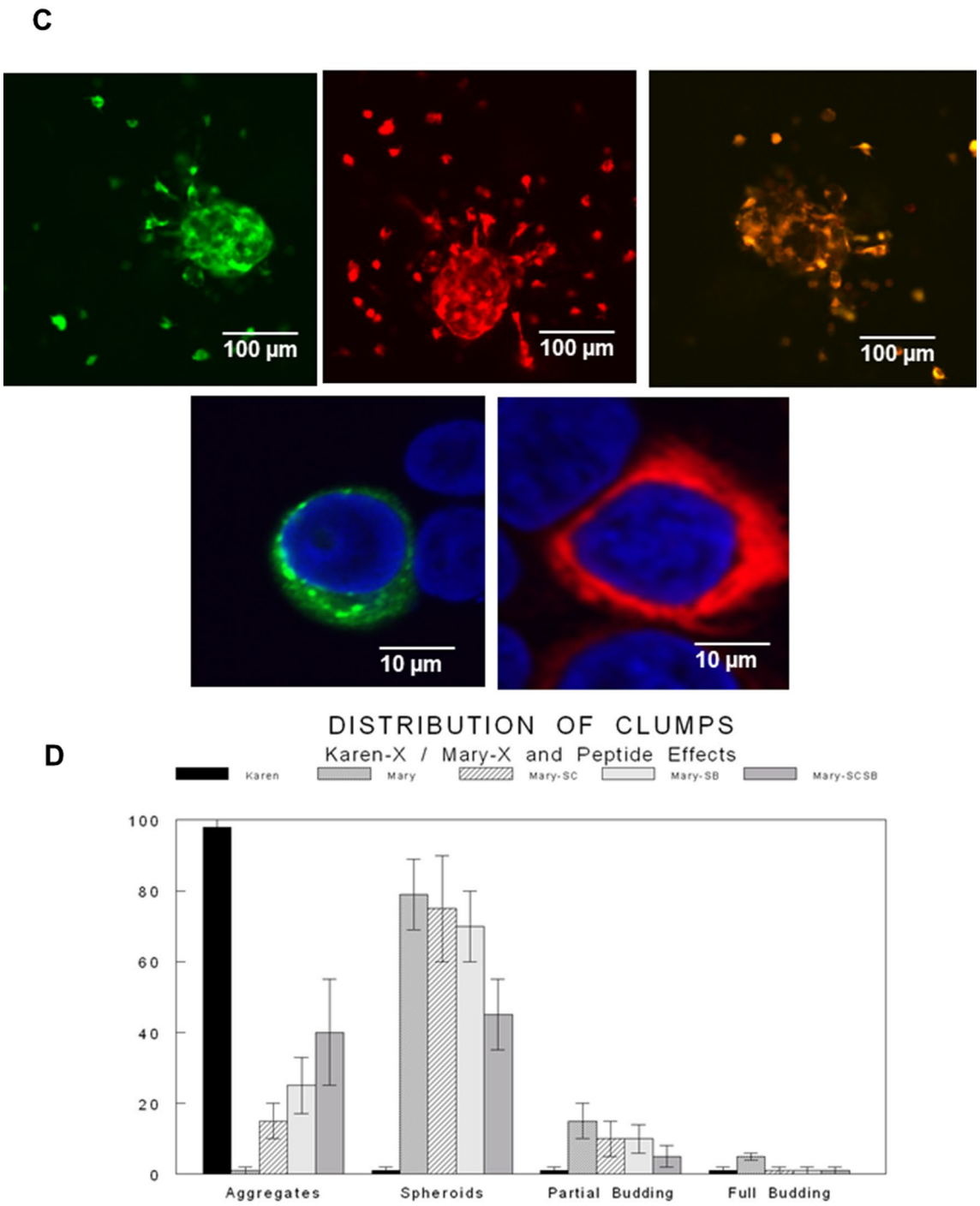

Fig. 6 (continued)

the 3D situation of in vivo cancer and to more faithfully recapitulate in vivo gene expression, provide better evaluation of physiological factors such as hypoxia and improved testing of anticancer pharmacological strategies. [51–53]

Most 3D models take the form of spheroids in suspension culture. The majority of these spheroids or multicellular aggregates (MTCs), however, need to be induced to grow as spheroids by growing them on agar or other repellent surface that interferes with the cancer cells natural proclivity to grow as monolayers. [54–63]

Some of these spheroids when injected into immunocompromised mice will develop into tumors but these tumors do not exhibit obvious lymphovascular invasion or tumor emboli formation. Furthermore no previous models have

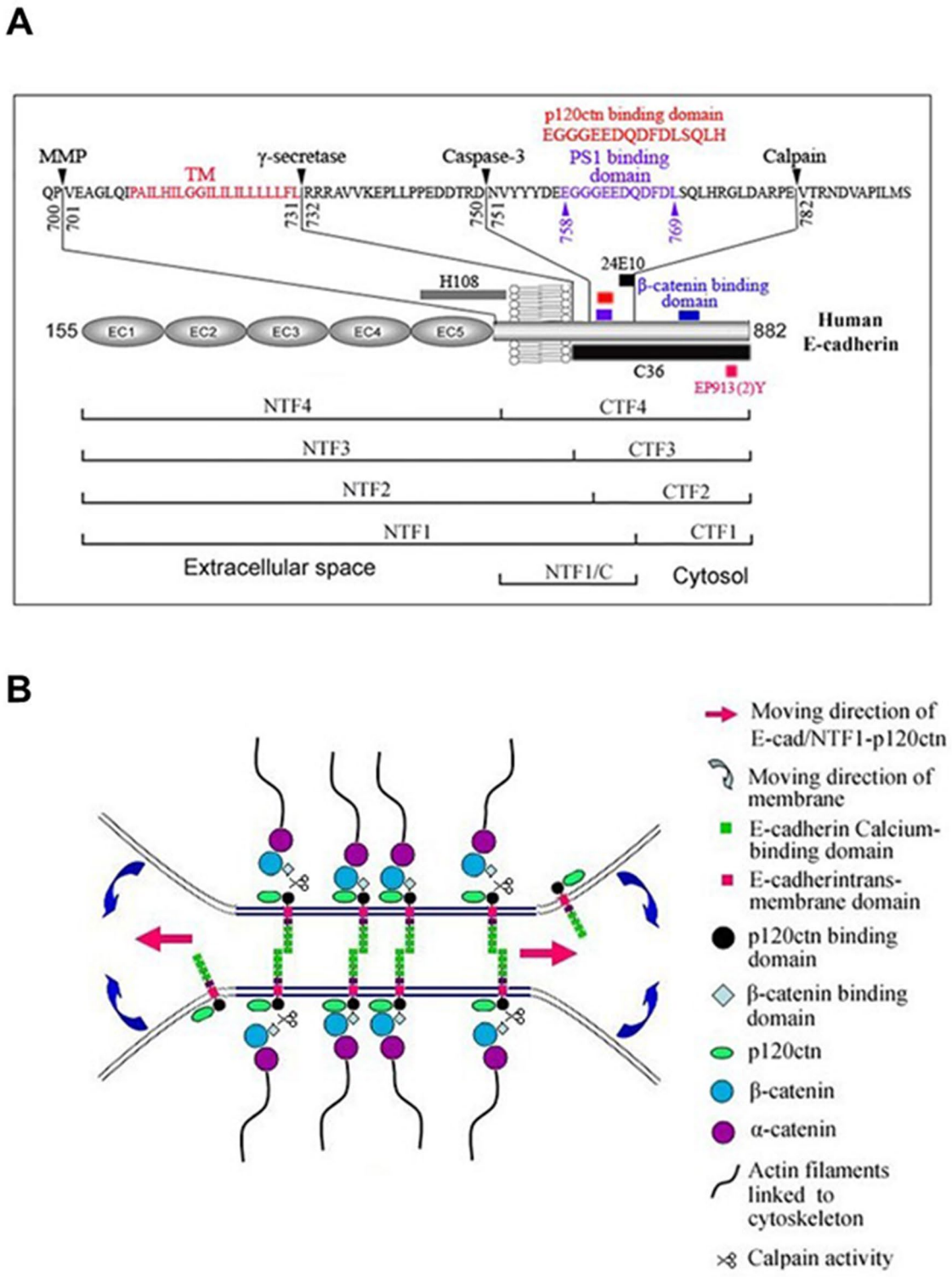

demonstrated the equivalence of in vitro spheroids with in vivo tumor emboli. In contrast, our in vitro spheroids of Mary-X *spontaneously* form and when re-injected into mice develop into tumors showing florid tumor emboli, which by Principal Component Analysis (PCA) not only express the transcriptome equivalence of Mary-X spheroids but also the equivalence of microdissected tumor emboli from cases of IBC [21, 30]. And the emboli of Mary-X and their in vitro equivalent, i.e., the spheroids are what undergo geometric budding.

◂**Fig. 7** Generation of E-cadherin and its fragments by different proteases. **A** Schematic (adapted by permission from Macmillan Publishers Ltd,; The EMBO Journal 2000; 21: 1948–1956, ref 71) depicts cleavage sites of calpain, caspase-3, MMP and γ-secretase including its obligate PS1 binding domain (highlighted) which is also thought to be the site of calpain binding as well and 8 of the E-cadherin fragments (E-cad/NTF1-4; E-cad/CTF1-4) generated by these specific cellular proteases. EC1-5 denote the extracellular E-cadherin repeats. TM indicates transmembrane domain (also highlighted). The sites of binding of two anti-E-cadherin antibodies, H108 and 24E10 are also depicted. Schematic adapted from Fig. 3, ref 71. **B** Schematic of E-cad/NTF1 membrane mobility depicts the structure of E-cad/NTF1 bound to p120ctn but not to β- or α-catenin nor the actin cytoskeleton. Therefore while E-cad/FL is tethered to the membrane in traditional CAJs, E-cad/NTF1 becomes more mobile, redistributing itself along adjacent areas of the membrane, contributing to increased budding

Although budding per se of tumor cells has also been observed and studied in vivo in other studies, that budding applies to invasion of the primary cancer and not specific budding of the lymphovascular tumor embolus [64–66]. Budding per se from the lymphovascular tumor embolus has not previously been observed or studied.

It is interesting that the hypothesis of EMT still dominates the thinking of the metastatic process even when applied to metastasizing clumps and budding where E-cadherin overexpression is also observed [46–48]; [67–69]. Despite this observation, the evidence suggests that the mechanism of budding responsible for geometric embolic propagation in our model does not involve either complete or partial EMT. Our time-lapsed photography indicates that complete in vitro budding occurs in minutes and that both the bud as well as the parent spheroid or embolus overexpress E-cadherin even at the incident point of budding. It makes more sense that budding results not from EMT followed by MET but rather from pre-existing molecules like E-cad/NTF1. Certainly budding must involve additional steps some of which could be energy (ATP) dependent, hypoxia triggered, nutrient-related or density regulated. We plan to use our budding model to delineate these steps in future studies.

Conclusions

Our study therefore is the first study that observes and quantitates actual budding of tumor emboli in an IBC model both in vivo and in vitro which account for the markedly greater number of tumor emboli and distinctly smaller emboli whose numbers reflect a geometric or exponential process in IBC patients.

Blocking the calpain-mediated proteolysis of membrane E-cadherin by SC and SB mimicking decapeptides suggests that E-cad/NTF1 participates in both tight spheroidgenesis as well as budding. E-cad/NFT1 retains its p120ctn binding site but loses both the β-catenin and α-binding sites, facilitating its disassembly from traditional CAJs. E-cad/NFT1 can exhibit 360° mobility around the membrane and its vacillating levels would both initiate and subsequently consolidate the budding process (Fig. 7B). This insight could lead to therapies at inhibiting budding and embolic propagation, thereby decreasing skin recurrences in IBC [70].

Supplementary Information The online version contains supplementary material available at https://doi.org/10.1007/s10549-022-06819-6.

Acknowledgements The authors wish to thank CUSM Instructional and Informational Technology Services for enabling videoconferencing coauthor communications during the COVID-19 pandemic. The authors further wish to thank Dean Burkin, PhD of the University of Nevada School of Medicine for advice concerning the oligopeptide studies.

Author Contributions All authors made an intellectual contribution to the work. Arnav P. Modi, carried out the vast majority of the in vitro spheroidgenesis and budding experiments. Julie P.T. Nguyen conducted a critical interpretation of the data and further characterized the nature of the budding. Justin Wang supervised the xenograft experiments. Jonathan S. Ahn analyzed the immunofluorescence and immunocytochemical experiments and conducted additional in vitro budding experiments. William A. Libling troubleshot additional experiments designed to test the significance of the hypothesis. Jacob M. Klein and Preeanka Mazumder conducted a review of the relevant literature and suggested additional experiments. Sanford H. Barsky supervised all of the experiments and wrote and further modified the manuscript which was reviewed by all the authors.

Funding This work was supported by the Department of Defense Breast Cancer Research Program Grants BC990959, BC024258, BC053405 and the Dr. Carolyn S. Glaubensklee Endowed Cancer Center Directorship.

Data Availability Both Mary-X and Karen-X are available to any investigator upon request. Imaging algorithms used in the study are also available. All data sets generated and used in the study are available upon request.

Declarations

Competing Interests The authors declare that they, at the present time, have no known competing financial interests or personal relationships that could have appeared to influence the work reported in this paper. None of the sources of support listed influenced the collection, analysis and interpretation of data, the generation of the hypothesis, the writing of the manuscript or the decision to submit the manuscript for publication.

Ethical Approval Initial xenograft studies were conducted under the UCLA's Human Subject Protection Committee and the Chancellor's Animal Research Committee (Certification 95–127-11). Continuing animal studies were approved by The Ohio State University's Animal Care and Use Committee (IACUC), protocol 2007A0218 and by The Ohio State University's Institutional Biosafety Committee, protocol 2007R0057. Additional animal studies were approved by the University of Nevada's School of Medicine and the Nevada Cancer Institute's IACUC, protocols 00439 and 00440 when the corresponding author of this study was affiliated with these previous institutions. Final animal studies were conducted under an Interinstitutional Agreement between the California University of Science and Medicine and Anticancer, Inc. using the latter's IACUC protocol D16-00503 and OLAW A3873-01.

Collection and use of human tissues from patients with breast cancer including non-IBC as well as IBC cases, completely anonymized, was approved by The Ohio State University Cancer IRB under protocol 2006C0042.

Consent for Publication Not applicable.

References

1. Dent R, Trudeau M, Pritchard KI, Hanna WM, Kahn HK, Sawka CA, Lickley LA, Rawlinson E, Sun P, Narod SA (2007) Triple-negative breast cancer: Clinical features and patterns of recurrence. Clin Cancer Res 13:4429–4434
2. Brenton JD, Carey LA, Ahmed A, Caldas C (2005) Molecular classification and molecular forecasting of breast cancer: Ready for clinical application? J Clin Oncol 23:7350–7360
3. Cristofanilli M, Buzdar AU, Hortobágyi GN (2003) Update on the management of inflammatory breast cancer; update on the management of inflammatory breast cancer. Oncologist 8:141–148
4. Kertmen N, Babacan T, Keskin O, Solak M, Sarici F, Akin S, Arik Z, Asian A, Ates O, Aksoy S, Ozisik Y, Altundag K (2015) Molecular subtypes in patients with inflammatory breast cancer. A single center experience J BUON 20:35–39
5. Alpaugh ML, Tomlinson JS, Shao ZM, Barsky SH (1999) A novel human xenograft model of inflammatory breast cancer. Cancer Res 59:5079–5084
6. Tomlinson JS, Alpaugh ML, Barsky SH (2001) An intact overexpressed E-cadherin/α, β-catenin axis characterizes the lymphovascular emboli of inflammatory breast carcinoma. Cancer Res 61:5231–5241
7. Alpaugh ML, Tomlinson JS, Ye Y, Barsky SH (2002) Relationship of sialyl-Lewisx/a underexpression and E-cadherin overexpression in the lymphovascular embolus of inflammatory breast carcinoma. Am J Pathol 161:619–628. https://doi.org/10.1016/S0002-9440(10)64217-4
8. Alpaugh ML, Tomlinson JS, Kasraeian S, Barsky SH (2002) Cooperative role of E-cadherin and sialyl-Lewis X/A-deficient MUC1 in the passive dissemination of tumor emboli in inflammatory breast carcinoma. Oncogene 21:3631–3643
9. Eckhardt BL, Gagliardi M, Iles LK, Evans K, Ivan C, Liu X, Liu CG, Souza G, Rao A, Meric-Bernstam F, Ueno NT, Bartholomeusz GA (2018) Clinically relevant inflammatory breast cancer patient-derived xenograft–derived ex vivo model for evaluation of tumor-specific therapies. PLoS ONE 13:1–23
10. Colpaert CG, Vermeulen PB, Benoy I, Soubry A, Van Roy F, Van Beest P, Goovaerts G, Dirix LY, Van Dam P, Fox SB, Harris AL, Van Marck EA (2003) Inflammatory breast cancer shows angiogenesis with high endothelial proliferation rate and strong E-cadherin expression. Br J Cancer 88:718–725
11. Ye Y, Tellez JD, Durazo M, Belcher M, Yearsley K, Barsky SH (2010) E-cadherin accumulation within the lymphovascular embolus of inflammatory breast cancer is due to altered trafficking. Anticancer Res 30:3903–3910
12. Alpaugh ML, Barsky SH (2002) Reversible model of spheroid formation allows for high efficiency of gene delivery Ex Vivo and accurate gene assessment In Vivo. Hum Gene Ther 13:1245–1258
13. Kalluri R, Weinberg RA (2009) The basics of epithelial-mesenchymal transition. J Clin Invest 119:1420–1428
14. Thiery JP, Acloque H, Huang RYJ, Nieto MA (2009) Epithelial-mesenchymal transitions in development and disease. Cell 139:871–890
15. Zheng X, Carstens JL, Kim J, Scheible M, Kaye J, Sugimoto H, Wu C, Lebleu VS, Kalluri R, Biology C (2015) EMT program is dispensable for metastasis but induces chemoresistance in pancreatic cancer. Nature 527:525–530
16. Fernandez SV, Robertson FM, Pei J, Aburto-Chumpitaz L, Mu Z, Chu K, Alpaugh RK, Huang Y, Cao Y, Ye Z, Cai KQ, Boley KM, Klein-Szanto AJ, Devarajan K, Addya S, Cristofanilli M (2013) Inflammatory breast cancer (IBC): Clues for targeted therapies. Breast Cancer Res Treat 140:23–33
17. Robertson FM, Bondy M, Yang W, Yamauchi H, Wiggins S, Kamrudin S, Krishnamurthy S, Le-Petross H, Bidaut L, Player AN, Barsky SH, Woodward WA, Buchholz T, Lucci A, Ueno N, Cristofanilli M (2010) Inflammatory breast cancer: the disease, the biology, the treatment. CA Cancer J Clin 60:351–375
18. Cristofanilli M, Valero V, Buzdar AU, Kau SW, Broglio KR, Gonzalez-Angulo AM, Sneige N, Islam R, Ueno NT, Buchholz TA, Singletary SE, Hortobagyi GN (2007) Inflammatory breast cancer (IBC) and patterns of recurrence: Understanding the biology of a unique disease. Cancer 110:1436–1444
19. Xiao Y, Ye Y, Yearsley K, Jones S, Barsky SH (2008) The lymphovascular embolus of inflammatory breast cancer expresses a stem cell-like phenotype. Am J Pathol 173:561–574
20. Xiao Y, Ye Y, Zou X, Jones S, Yearsley K, Shetuni B, Tellez J, Barsky SH (2011) The lymphovascular embolus of inflammatory breast cancer exhibits a Notch 3 addiction. Oncogene 30:287–300
21. Ye Y, Tian H, Lange AR, Yearsley K, Robertson FM, Barsky SH (2013) The genesis and unique properties of the lymphovascular tumor embolus are because of calpain-regulated proteolysis of E-cadherin. Oncogene 32:1702–1713
22. Sharangpani GM, Joshi AS, Porter K, Deshpande AS, Keyhani S, Naik GA, Gholap AS, Barsky SH (2007) Semi-automated imaging system to quantitate estrogen and progesterone receptor immunoreactivity in human breast cancer. J Microsc 226:244–255
23. Joshi AS, Sharangpani GM, Porter K, Keyhani S, Morrison C, Basu AS, Gholap GA, Gholap AS, Barsky SH (2007) Semi-automated imaging system to quantitate Her-2/neu membrane receptor immunoreactivity in human breast cancer. Cytom Part A 71A:273–285
24. Barsky SH, Gentchev L, Basu AS, Jimenez RE, Boussaid K, Gholap AS (2009) Use and validation of epithelial recognition and fields of view algorithms on virtual slides to guide TMA construction. Biotechniques 47:927–938
25. Mahooti S, Porter K, Alpaugh ML, Ye Y, Xiao Y, Jones S, Tellez JD, Barsky SH (2010) Breast carcinomatous tumoral emboli can result from encircling lymphovasculogenesis rather than lymphovascular invasion. Oncotarget 1:131–147
26. Gholap AS, Gholap GA, Rao CVK, Barsky SH, Vipra M, Patil SM, Jadhav P, Abhyankar J. Methods and system for morphology based mitoses identification and classification of digital images. U.S. Patent 7,979,212; July 12, 2–11.
27. Petrova SC, Ahmad I, Nguyen C, Ferrell SD Jr, Wilhelm SR, Ye Y, Barsky SH (2020) Regulation of breast cancer oncogenesis by the cell of origin's differentiation state. Oncotarget 11(43):3832–3848. https://doi.org/10.18632/oncotarget.27783
28. https://ij.imjoy.io
29. Grover PK, Cummins AG, Price TJ, Roberts-Thomson IC, Hardingham JE (2014) Circulating tumour cells: The evolving concept and the inadequacy of their enrichment by EpCAM-based methodology for basic and clinical cancer research. Ann Oncol 25:1506–1516
30. Ye Y, Gao JX, Tian H, Yearsley K, Lange AR, Robertson FM, Barsky SH (2012) Early to intermediate steps of tumor embolic formation involve specific proteolytic processing of E-cadherin regulated by Rab7. Mol Cancer Res 10(6):713–726. https://doi.org/10.1158/1541-7786.MCR-12-0009
31. Yamauchi H, Woodward WA, Valero V, Alvarez RH, Lucci A, Buchholz TA, Iwamoto T, Krishnamurthy S, Yang W, Reuben

JM, Hortobágyi GN, Ueno NT (2012) Inflammatory breast cancer: what we know and what we need to learn. Oncologist 17:891–899
32. Patani N, Mokbel K (2008) Oncological and aesthetic considerations of skin-sparing mastectomy. Breast Cancer Res Treat 111:391–403
33. Hoffman DI, Santos PMG, Goldbach M, Keele LJ, Taunk NK, Bogen HS, Burkbauer L, Jankowitz RC, Fosnot J, Wu LC, Freedman GM, Tchou JC (2021) Immediate breast reconstruction for inflammatory breast cancer: trends in use and clinical outcomes 2004–2016. Ann Surg Oncol 28:8789–8801
34. Norhisham NF, Chong CY, Safuan S (2017) Peritumoral lymphatic vessel density and invasion detected with immunohistochemical marker D240 is strongly associated with distant metastasis in breast carcinoma. BMC Clin Pathol, BMC Clinical Pathology 17:1–7
35. Kong L-L, Yang N-Z, Shi L-H, Zhao G-H, Zhou W, Ding Q, Wang M-H, Zhang Y-S (2017) The optimum marker for the detection of lymphatic vessels. Mol Clin Oncol 7:515–520
36. Lozar T, Gersak K, Cemazar M, Kuhar CG, Jesenko T (2019) The biology and clinical potential of circulating tumor cells. Radiol Oncol 53(2):131–147. https://doi.org/10.2478/raon-2019-0024
37. Wong SY, Hynes RO (2006) Lymphatic or hematogenous dissemination: how does a metastatic tumor cell decide? Cell Cycle 5(8):812–817. https://doi.org/10.4161/cc.5.8.2646
38. Lambert AW, Pattabiraman DR, Weinberg RA (2017) Emerging biological principles of metastasis. Cell 168(4):670–691. https://doi.org/10.1016/j.cell.2016.11.037
39. Hidalgo M, Amant F, Biankin AV, Budinská E, Byrne AT, Caldas C, Clarke RB, de Jong S, Jonkers J, Mælandsmo GM, Roman-Roman S, Seoane J, Trusolino L, Villanueva A (2014) Patient-derived xenograft models: an emerging platform for translational cancer research. Cancer Discov 4(9):998–1013
40. Yin L, Wang XJ, Chen DX, Liu XN, Wang XJ (2020) Humanized mouse model: a review on preclinical applications for cancer immunotherapy. Am J Cancer Res 10(12):4568–4584
41. Chernofsky MR, Felix JC, Muderspach LI, Morrow CP, Ye W, Groshen SG, Roman LD (2006) Influence of quantity of lymph vascular space invasion on time to recurrence in women with early-stage squamous cancer of the cervix. Gynecol Oncol 100:288–293
42. Sykes P, Allen D, Cohen C, Scurry J, Yeo D (2003) Does the density of lymphatic vascular space invasion affect the prognosis of stage Ib and IIA node negative carcinoma of the cervix? Int J Gynecol Cancer 13:313–316
43. Roman LD, Felix JC, Muderspach LI, Varkey T, Burnett AF, Qian D, Morrow CP (1998) Influence of quantity of lymph-vascular space invasion on the risk of nodal metastases in women with early-stage squamous cancer of the cervix. Gynecol Oncol 68:220–225
44. Scurry J, Hacker NF, Barlow E, Friedlander M, Jackson M (2015) Is quantification of lymphovascular space invasion useful in stage 1B2 cervical carcinomas? J Obstet Gynaecol (Lahore) 35:377–381
45. Jolly MK, Boareto M, Debeb BG, Aceto N, Farach-Carson MC, Woodward WA, Levine H (2017) Inflammatory breast cancer: A model for investigating cluster-based dissemination. Breast Cancer 3:1–7. https://doi.org/10.1038/s41523-017-0023-9
46. Somarelli JA, Schaeffer D, Marengo MS, Bepler T, Rouse D, Ware KE, Hish AJ, Zhao Y, Buckley AF, Epstein JI, Armstrong AJ, Virshup DM, Garcia-Blanco MA (2016) Distinct routes to metastasis: Plasticity-dependent and plasticity-independent pathways. Oncogene 35:4302–4311. https://doi.org/10.1038/onc.2015.497
47. Aceto N, Bardia A, Miyamoto DT, Donaldson MC, Wittner BS, Spencer JA, Yu M, Pely A, Engstrom A, Zhu H, Brannigan BW, Kapur R, Stott SL, Shioda T, Ramaswamy S, Ting DT, Lin CP, Toner M, Haber DA, Maheswaran S (2014) Circulating tumor cell clusters are oligoclonal precursors of breast cancer metastasis. Cell 158:1110–1122. https://doi.org/10.1016/j.cell.2014.07.013
48. Cheung KJ, Padmanaban V, Silvestri V, Schipper K, Cohen JD, Fairchild AN, Gorin MA, Verdone JE, Pienta KJ, Bader JS, Ewald AJ (2016) Polyclonal breast cancer metastases arise from collective dissemination of keratin 14-expressing tumor cell clusters. Proc Natl Acad Sci U S A 113:E854–E863
49. Choi YJ, Pinto MM, Hao L, Riba AK (2008) Interobserver variability and aberrant E-cadherin immunostaining of lobular neoplasia and infiltrating lobular carcinoma. Mod Pathol 21:1224–1237
50. Palacios J, Sarrió D, García-Macias MC, Bryant B, Sobel ME, Merino MJ (2003) Frequent E-cadherin gene inactivation by loss of heterozygosity in pleomorphic lobular carcinoma of the breast. Mod Pathol 16:674–678
51. Weiswald LB, Bellet D, Dangles-Marie V (2015) Spherical cancer models in tumor biology. Neoplasia (United States) 17:1–15. https://doi.org/10.1016/j.neo.2014.12.004
52. Zanoni M, Piccinini F, Arienti C, Zamagni A, Santi S, Polico R, Bevilacqua A, Tesei A (2016) 3D tumor spheroid models for in vitro therapeutic screening: A systematic approach to enhance the biological relevance of data obtained. Sci Rep 6:1–11. https://doi.org/10.1038/srep19103
53. Nath S, Devi GR (2016) Three-dimensional culture systems in cancer research: Focus on tumor spheroid model. Pharmacol Ther 163:94–108
54. Young SR, Saar M, Santos J, Nguyen HM, Vessella RL, Peehl DM (2013) Establishment and serial passage of cell cultures derived from LuCaP xenografts. Prostate 73:1251–1262
55. Oktem G, Sercan O, Guven U, Uslu R, Uysal A, Goksel G, Ayla S, Bilir A (2014) Cancer stem cell differentiation: TGFβ1 and versican may trigger molecules for the organization of tumor spheroids. Oncol Rep 32:641–649
56. Froehlich K, Haeger JD, Heger J, Pastuschek J, Photini SM, Yan Y, Lupp A, Pfarrer C, Mrowka R, Schleußner E, Markert UR, Schmidt A (2016) Generation of multicellular breast cancer tumor spheroids: comparison of different protocols. J Mammary Gland Biol Neoplasia 21:89–98
57. Arora J, Sauer SJ, Tarpley M, Vermeulen P, Rypens C, Van LS, Williams KP, Devi GR, Dewhirst MW (2017) Inflammatory breast cancer tumor emboli express high levels of anti-apoptotic proteins: Use of a quantitative high content and high-throughput 3D IBC spheroid assay to identify targeting strategies. Oncotarget 8:25226–25241
58. Kang HG, Jenabi JM, Zhang J, Keshelava N, Shimada H, May WA, Ng T, Reynolds CP, Triche TJ, Sorensen PHB (2007) E-cadherin cell-cell adhesion in Ewing tumor cells mediates suppression of anoikis through activation of the ErbB4 tyrosine kinase. Cancer Res 67:3094–3105
59. Van Golen KL, Wu ZF (2000) Xiao Tan Qiao, Li Wei Bao, Merajver SD: RhoC GTPase, a novel transforming oncogene for human mammary epithelial cells that partially recapitulates the inflammatory breast cancer phenotype. Cancer Res 60:5832–5838
60. Weiswald LB, Richon S, Massonnet G, Guinebretière JM, Vacher S, Laurendeau I, Cottu P, Marangoni E, Nemati F, Validire P, Bellet D, Bièche I, Dangles-Marie V (2013) A short-term colorectal cancer sphere culture as a relevant tool for human cancer biology investigation. Br J Cancer 108:1720–1731
61. Weiswald LB, Richon S, Validire P, Briffod M, Lai-Kuen R, Cordelières FP, Bertrand F, Dargere D, Massonnet G, Marangoni E, Gayet B, Pocard M, Bieche I, Poupon MF, Bellet D, Dangles-Marie V (2009) Newly characterised ex vivo colospheres as a three-dimensional colon cancer cell model of tumour aggressiveness. Br J Cancer 101:473–482
62. Kondo J, Endo H, Okuyama H, Ishikawa O, Iishi H, Tsujii M, Ohue M, Inoue M (2011) Retaining cell-cell contact enables preparation and culture of spheroids composed of pure primary

cancer cells from colorectal cancer. Proc Natl Acad Sci U S A 108:6235–6240
63. Lehman HL, Dashner EJ, Lucey M, Vermeulen P, Dirix L, Van LS, Van Golen KL (2013) Modeling and characterization of inflammatory breast cancer emboli grown in vitro. Int J Cancer 132:2283–2294
64. Dawson H, Lugli A (2015) Molecular and pathogenetic aspects of tumor budding in colorectal cancer. Front Med 2:11
65. Man Y (2010) gao: Tumor cell budding from focally disrupted tumor capsules: A common pathway for all breast cancer subtype derived invasion. J Cancer 1:32–37
66. Pease JC, Brewer M, Tirnauer JS (2012) Spontaneous spheroid budding from monolayers: A potential contribution to ovarian cancer dissemination. Biol Open 1:622–628
67. Bronsert P, Enderle-Ammour K, Bader M, Timme S, Kuehs M, Csanadi A, Kayser G, Kohler I, Bausch D, Hoeppner J, Hopt UT, Keck T, Stickeler E, Passlick B, Schilling O, Reiss CP, Vashist Y, Brabletz T, Berger J, Lotz J, Olesch J, Werner M, Wellner UF (2014) Cancer cell invasion and EMT marker expression: a three-dimensional study of the human cancer-host interface. J Pathol 234:410–422
68. Grigore A, Jolly M, Jia D, Farach-Carson M, Levine H (2016) Tumor budding: the name is EMT. Partial EMT J Clin Med 5:51
69. Boareto M, Jolly MK, Goldman A, Pietilä M, Mani SA, Sengupta S, Ben-Jacob E, Levine H, Onuchic JN (2016) Notch-Jagged signalling can give rise to clusters of cells exhibiting a hybrid epithelial/mesenchymal phenotype. J R Soc Interface. https://doi.org/10.1098/rsif.2015.1106
70. Dobiasova B, Mego M (2020) Biomarkers for inflammatory breast cancer: Diagnostic and therapeutic utility. Breast Cancer Targets Ther 12:153–163
71. Marambaud P, Shioi J, Serban G, Georgakopoulos A, Sarner S, Nagy V, Baki L, Wen P, Efthimiopoulos S, Shao Z, Wisniewski T, Robakis NK (2002) A presenilin-1/gamma-secretase cleavage releases the E-cadherin intracellular domain and regulates disassembly of adherens junctions. EMBO J 21(8):1948–1956. https://doi.org/10.1093/emboj/21.8.1948